

FPGA-based Adaptive Notch Filters for the Active Cancellation of Varying Electromagnetic Emissions of Power Electronic Inverter Systems

Tobias Dörlemann, Andreas Bendicks, Stephan Frei
On-board Systems Lab
TU Dortmund University
Dortmund, Germany
tobias.doerlemann@tu-dortmund.de

Abstract—In many modern power electronic systems, fast-switching semiconductor devices are used to reduce switching losses. Due to steep switching waveforms and high switching frequencies, significant electromagnetic disturbances can be emitted. In contrast to conventional passive filter components, active cancellation methods are based on the controlled destructive interference between a noise signal and a corresponding anti-noise signal. Adaptive notch filters revealed themselves as a promising active EMI cancellation concept for periodic noise signals. In this work, adaptive notch filters are regarded in context of slowly time-varying periodic noise signals, e.g. pulse-width modulated signals as common in inverters. The corresponding noise signals consist of switching harmonics and adjacent sideband harmonics. Therefore, the notch filter’s bandwidth comes into focus and an analytical approximation for the ideal adaptive notch filter’s bandwidth is discussed. With help of this approximation, the adaptive notch filter can be parametrized specifically to a given noise spectrum and other requirements. The capability of the parametrization strategy and the adaptive notch filter itself are shown by simulation and measurement.

Keywords—power electronics, inverter, electromagnetic emissions, adaptive notch filter, active cancellation

I. INTRODUCTION

Fast-switching power electronic converters are relevant sources of electromagnetic interferences (EMI). Conventionally, passive filter components are used to reduce this EMI and to comply with international standards on electromagnetic compatibility (EMC) [1], e.g., CISPR 25 for vehicles [2]. One idea to reduce weight and volume of these passive filter structures is to make use of active EMI filtering concepts [3-5]. These concepts in general aim for a destructive interference between noise and anti-noise signals.

To yield a complete destructive interference, the anti-noise signal must equal the noise signal with opposite sign. Therefore, in feedback active filtering concepts, noise signals are measured, inverted, amplified and back-injected as anti-noise signals. Due to unavoidable signal propagation delays and time constants in implementations of these concepts, the perfect fit of phases between noise and anti-noise signals is limited and, thereby, also the achievable noise suppression [6].

By injecting synthesized and synchronized anti-noise signals, the limiting influence of time constants and signal propagation delays can be compensated. In [7], the needed anti-noise signal is calculated by identifying the noise signal with help of an off-line fast fourier transform (FFT) and consideration of the transmission path’s influence on the injected cancellation signal. Due to the needed calculation time, this method assumes periodicity of the noise signal and

absolutely precise synchronization between the noise and the anti-noise sources. Today only cancellation systems using the digital clock of the noise system can provide the needed synchronicity.

In contrast, the fundamental idea of an adaptive notch filter is the synthesis, injection and continuous adaptation of a single sinusoidal signal in amplitude and phase for every noise signal frequency to be mitigated. Hereby, time constants, propagation delays and slight variations of the noise can be compensated. By applying multiple notch filters in parallel and superposing all anti-noise signals, noise signals consisting of multiple undesired frequencies can be mitigated.

With help of adaptive notch filter implementations and inspired by previous investigations in the acoustics domain [8], an FPGA-based adaptive EMI cancellation strategy is presented to mitigate the switching harmonics of a stationary operating DC-to-DC-converter in [9]. Due to the artificial synthesis and the continuous adaptation of the anti-noise signal’s amplitude and phase, high noise reductions can be achieved for periodic narrowband noise signals.

In [10, 11], adaptive notch filter implementations have been applied to a power factor correction (PFC). Due to the pulse-width-modulated (PWM) control scheme, the corresponding EMI consists of numerous switching harmonics with adjacent sideband harmonics. As shown in [11], these sidebands around the switching harmonics correspond to modulated sine waves in time domain. Assuming a sufficiently fast adaptation speed, these modulated sine waves can be suppressed with help of adaptive notch filter implementations. Because a too fast adaptation speed can lead to instability, a systematic parametrization of the adaptive notch filter is needed.

In this work, an analysis of the ideal adaptive notch filter’s behavior is presented. Based on this analysis, a systematic parametrization strategy for the adaptive notch filter’s step size – that is essentially influencing the adaptation speed – is elaborated. The suitability of this parametrization strategy is examined by simulation and with help of a simplified test setup as an emulation for an inverter.

II. SPECTRUM OF A MODULATED PWM-SIGNAL

In Fig. 1, a simple inverter model and a switching waveform of a sinusoidally modulated PWM-signal in time domain (right upper plot) are shown. The modulated PWM-signal is found by comparing a sawtooth-carrier signal with frequency f_C with a sinusoidal reference signal with frequency f_{Ref} . The corresponding spectrum is illustrated in the right lower plot of Fig. 1. Due to the pulse-width modulation, sideband harmonics occur and are spaced in

distance of multiples of f_{Ref} . The low-frequency sinusoidal modulation keeps the subharmonics close to the harmonics. The harmonic frequencies are slightly increased or decreased. The adaptive notch filter can follow well such slow changes [12].

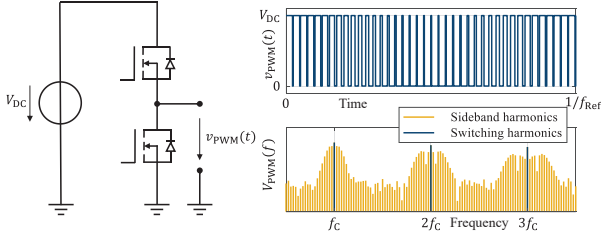


Fig. 1. Simple half-bridge inverter model (left) with pulse-width modulated switching waveform, Illustration of a PWM signal and an extract of its spectrum (right)

III. ADAPTIVE NOTCH FILTER ALGORITHM

Adaptive notch filters have been extensively examined in acoustics e.g. [8, 14-16] as a promising concept for active noise cancellation and can be classified as narrowband feedforward active noise control (ANC) systems. In previous works, the application of adaptive notch filters to mitigate periodic EMI signals revealed to be a promising approach in the field of active EMI cancellation, e.g. [9, 10, 11, 12, 13].

A. Ideal Adaptive Notch Filter Behavior

In Fig. 2, a time-discrete single-frequency adaptive notch filter algorithm is depicted. An arbitrary time-discrete cosine signal $x_0(n)$ and an arbitrary time-discrete sine signal $x_1(n)$ with frequency f_0 are synthesized in parallel. Both signals are multiplied with a weighting factor $w_0(n)$ and $w_1(n)$ before the resulting products $x_0(n) \cdot w_0(n)$ and $x_1(n) \cdot w_1(n)$ are superimposed. By adapting the filter weights in every single sample time with help of the Least Mean Square (LMS) algorithm, the resulting anti-noise signal $y(n)$ can be adjusted in amplitude and phase (1).

$$w_{0,1}(n+1) = w_{0,1}(n) + \mu \cdot e(n) \cdot x_{0,1}(n) \quad (1)$$

This adaptation process with high time resolution is based on the measurement of the residual noise signal $e(n)$ that results from the superposition of the noise and anti-noise signal. The step size μ determines the adaptation and convergence speed of the algorithm. A small step size causes a slow adaptation, a bigger step size directs a faster adaptation.

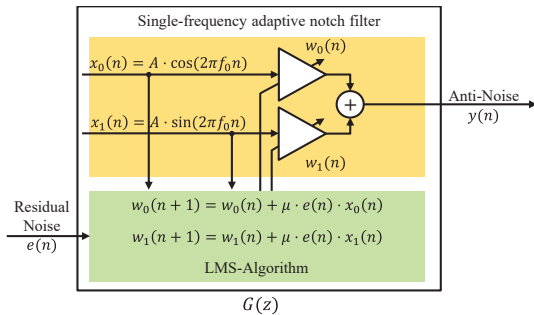


Fig. 2. Single-frequency adaptive notch filter with LMS algorithm

As shown in e.g. [14, 15, 16], the adaptive notch filter shown in Fig. 2 can be modeled by a time-discrete transfer function $G(z)$ with sample time T_s . This transfer function describes the relationship between the residual noise signal $e(n)$ as the notch filter's input and the anti-noise signal $y(n)$ as the notch filter's output signal. This linear time-invariant notch filter model is valid after a transient adaptation time [16].

$$G(z) = \frac{Y(z)}{E(z)} \approx \frac{\mu A^2 \cdot (z \cdot \cos(2\pi f_0 T_s) - 1)}{z^2 - 2z \cdot \cos(2\pi f_0 T_s) + 1} \quad (2)$$

As depicted in Fig. 3, the superposition of the noise signal $d(n)$ and the anti-noise signal $y(n)$ leads to the residual noise signal $e(n)$.

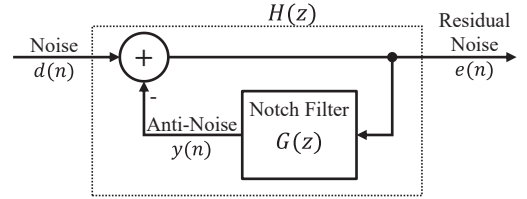


Fig. 3. Block diagram representation of notch filter configuration

The corresponding closed-loop transfer function $H(z)$ in (3) describes the relationship between the noise signal $d(n)$ and the residual noise signal $e(n)$ [14, 15, 16].

$$H(z) = \frac{E(z)}{D(z)} = \frac{1}{1+G(z)} = \frac{z^2 - 2z \cdot \cos(2\pi f_0 T_s) + 1}{z^2 - (2 - \mu A^2)z \cdot \cos(2\pi f_0 T_s) + 1 - \mu A^2} \quad (3)$$

With help of $H(z)$, the ideal adaptive notch filter's behavior can be analyzed and the expectable noise reduction over frequency can be calculated. The characteristic notch can be visualized by depicting the magnitude of $H(z)$ over frequency, as shown in Fig. 5.

As shown in detail in [14, 15, 16], the poles of $H(z)$ for $\mu A^2/2 \ll 1$ are approximately equal to (4).

$$z_{\text{pole}} \approx \left(1 - \frac{\mu A^2}{2}\right) \cdot e^{\pm j 2\pi f_0 T_s} \quad (4)$$

For stability, the poles have to lie inside the unit circle. Therefore, from (4), the following stability condition of $H(z)$ for μ can be derived and is given in (5).

$$0 < \mu < \frac{2}{A^2} \quad (5)$$

The zeros of $H(z)$ are lying on the unit circle, as expressed in (6). Hence, the frequency f_0 describes the ideal notch filter's center frequency with infinite noise suppression.

$$z_{\text{zero}} = e^{\pm j 2\pi f_0 T_s} \quad (6)$$

The characteristic notch around the center frequency is determined by the closeness of the poles to the zeros [14, 16] as illustrated in Fig. 4. In [15], the 3-dB bandwidth of the ideal filter notch is geometrically determined by finding the two points on the z -plane's unit circle which are $\sqrt{2}$ times as far away from a pole as they are from the corresponding zero.

In an analogous manner, the corresponding bandwidth of a higher noise suppression X_{dB} can be approximated by finding the two points z_1, z_2 on the z -plane's unit circle that are $10^{\frac{X_{\text{dB}}}{20}}$ times as far away from a pole as they are from the corresponding zero. In Fig. 4, these points z_1, z_2 are marked by the grey dots on the unit circle. Their distance a to the zero can be calculated using the Pythagorean theorem, and results in (7).

$$a = \frac{\mu A^2}{2} \cdot \sqrt{\frac{1}{10^{\left(\frac{X_{\text{dB}}}{10 \text{ dB}}\right)} - 1}} \quad (7)$$

For a small angle $\Delta\varphi$ between z_1 and z_{zero} in the unit circle and with help of the sinusoid's small-angle approximation, $\Delta\varphi$ equals approximately a . The searched notch bandwidth corresponds to this small angle $\Delta\varphi$ as shown in (8).

$$\Delta\varphi = 2\pi \frac{B_{X_{\text{dB}}}}{2} T_s \quad (8)$$

With help of (7) and $\Delta\varphi \approx a$, the searched notch bandwidth in Hz can be approximated as shown in (9).

$$B_{X_{\text{dB}}} \approx \frac{\mu A^2}{2\pi T_s} \cdot \sqrt{\frac{1}{10^{\left(\frac{X_{\text{dB}}}{10 \text{ dB}}\right)} - 1}} \quad (9)$$

Finally, (9) can be rearranged to (10) which allows the calculation of the needed step size μ for a demanded X_{dB} - bandwidth $B_{X_{\text{dB}}}$ and a required suppression of X_{dB} .

$$\mu \approx B_{X_{\text{dB}}} \cdot \frac{2\pi T_s}{A^2} \cdot \frac{1}{\sqrt{\frac{1}{10^{\left(\frac{X_{\text{dB}}}{10 \text{ dB}}\right)} - 1}}} \quad (10)$$

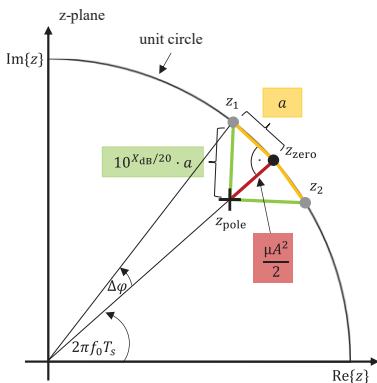


Fig. 4. Cutout of the z -plane's unit circle

In Fig. 5, two filter notches for two exemplary step sizes μ are visualized. The vertical grey marks depict the corresponding -15 dB-bandwidth ($X_{\text{dB}} = 15$ dB, $A = 1$, $T_s = 8$ ns, $f_0 = 100$ kHz) which is analytically approximated with help of (9). Obviously, a bigger step size μ leads to a wider filter notch and therefore allows the suppression of wider noise signal frequency bands.

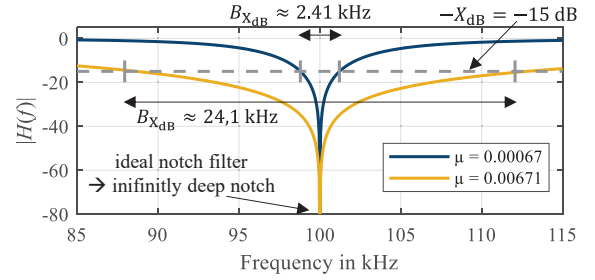


Fig. 5. Filter notches for two exemplarily chosen step sizes μ

B. Real Adaptive Notch Filter Implementations

In contrast to the ideal notch filter model in Fig. 2 and Fig. 3, the anti-noise signal is not directly superimposed with the noise signal in real adaptive notch filter implementations. In practice, the notch filter implementation can be realized by, e.g., an FPGA. In this case, there are, e.g., time delays by ADCs, DACs, injecting and measuring circuits that influence the real adaptive notch filter's behavior. In [8, 16], these effects are modeled by a secondary path transfer function $S(z)$. To compensate for the corresponding delays, the LMS algorithm is implemented as a delayed-LMS (DLMS) algorithm as shown in Fig. 6 [16, 17]. With help of the artificial delay Δ , which is an estimation of the secondary path's phase delay [16], the reference signal is aligned to the corresponding residual noise signal to ensure stability. Besides, the estimation Δ has to lead to a phase error, smaller than $\pm 90^\circ$ [8].

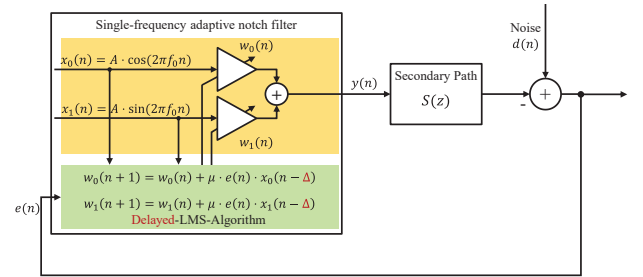


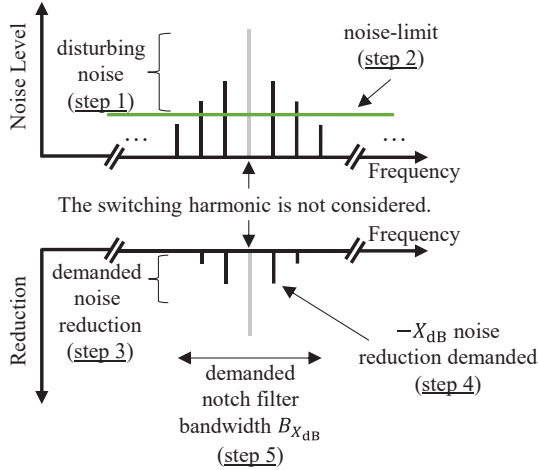
Fig. 6. Single-frequency adaptive notch filter with delayed-LMS algorithm

IV. PARAMETRIZATION STRATEGY

The proposed notch filter parametrization strategy bases on the following steps and is illustrated in Fig. 7:

1. Determination of the noise spectrum
2. Determination of a noise-limit
3. Calculation of the demanded noise reduction in dB by subtracting the noise-limit and the noise level of the regarded sideband. Only those sideband harmonics are considered that exceed the noise limit.
4. The demanded noise reduction X_{dB} is chosen as the maximum demanded noise reduction of the sideband (switching harmonic excluded).
5. The demanded notch filter bandwidth $B_{X_{\text{dB}}}$ is chosen as the frequency span between the first outer sideband harmonics that do not require noise reduction.
6. The needed notch filter bandwidth is calculated using (10).

In the following, this parametrization strategy is tested with help of simulations and measurements.



Calculation of the needed Notch Filter step size μ (step 6).

Fig. 7. Illustration of the proposed parametrization strategy

V. SIMULATION

To demonstrate and verify the proposed parametrization strategy, selected simulation-based examples are shown in the following. At first, a sawtooth carrier signal with carrier frequency $f_C = 100$ kHz and a sinusoidal reference signal with frequency $f_{Ref} = 50$ Hz are compared to calculate a binary PWM-signal. In the next step, the FFT of the PWM signal is calculated to evaluate the noise signal's sidebands at 100 kHz, 1 MHz and 10 MHz.

Based on an arbitrarily chosen maximum noise level in the frequency range of the considered switching harmonic and its sideband harmonics, the needed notch filter step size μ and the needed bandwidth are calculated. In the next step, an ideal notch filter model is parametrized with this step size μ and the corresponding residual noise signal is simulated.

A. Simulation of the noise spectrum

At first, the noise signal's FFT is calculated. In Fig. 9, the noise signal's sidebands around the switching harmonics 100 kHz, 1 MHz and 10 MHz are depicted (blue). In addition to that, maximum noise levels for the regarded sideband are arbitrarily chosen. In Fig. 9, these limits are visualized by a green horizontal line.

B. Parametrization

Based on the calculated noise spectra (step 1) and the arbitrarily chosen noise limits (step 2), the demanded noise reductions for the three different noise signal sidebands are calculated by subtracting the noise limit in $\text{dB}\mu\text{V}$ and the sideband's noise levels in $\text{dB}\mu\text{V}$ (step 3). Only those sideband frequency components are considered that exceed the noise limit. In Fig. 8, the resulting demanded reductions over frequency are depicted for the three different sidebands and the corresponding limits. Moreover, the maximum needed noise reductions for sideband harmonics (the switching harmonic is excluded) X_{dB} (step 4) and the sideband bandwidths (step 5) are marked. Based on these parameters and with help of (10), the needed step size μ is calculated

(step 6). The magnitude over frequency of the corresponding ideal notch filter transfer function $H(z)$ is depicted in Fig. 8, to illustrate the basic idea of the notch filter parametrization concept.

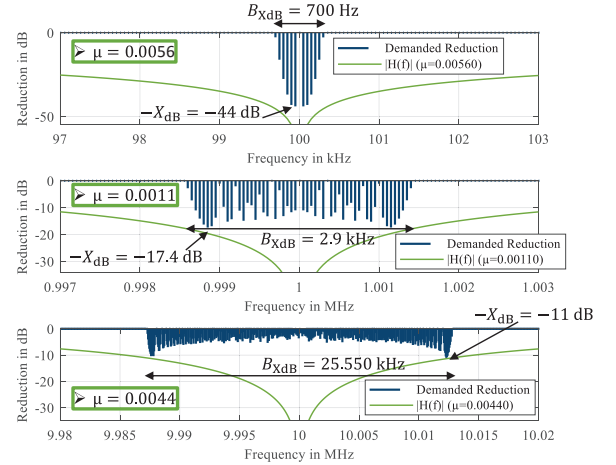


Fig. 8. Demanded noise reductions (blue), Magnitude of the ideal notch filter's transfer function for the parametrized step size μ (green)

C. Simulated noise reduction

After the needed step sizes are calculated for the given parameter set, the ideal notch filter behavior is simulated with help of a MATLAB model. The resulting residual noise spectra, the noise signal's sidebands and the requirements are shown in Fig. 9 for the three regarded sideband spectra. It can be summarized that all three simulated residual noise sidebands comply with the given requirements.

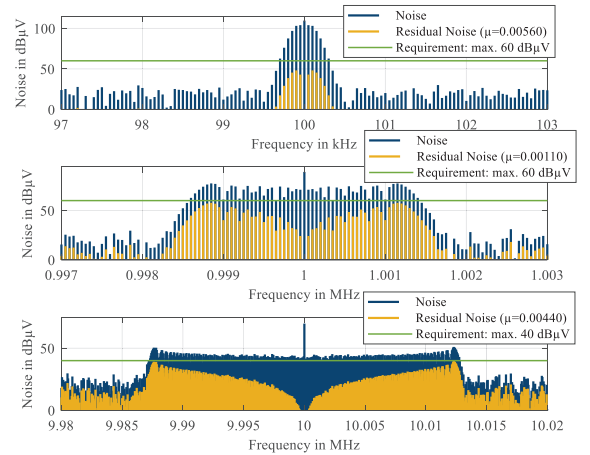


Fig. 9. Comparison of noise and residual-noise spectra

VI. MEASUREMENT

To test the described parametrization strategy and to emulate an inverter's switching waveform with help of a simple test setup, an FPGA-development board Red Pitaya STEMLab 125-14 is used to calculate a PWM signal and as a hardware basis for the adaptive notch filter implementation. With help of fast Analog-to-Digital and Digital-to-Analog Converters (125 MS/s), this FPGA-development board is able

to measure and synthesize signals in the desired frequency range.

The FPGA implementation emulates an inverter's switching waveform by comparing a 100 kHz sawtooth carrier with a 50 Hz reference sinusoid. This PWM signal is injected as a noise signal into a simple power splitter test setup as depicted in Fig. 10. The FPGA implementation also comprises an adaptive notch filter with delayed-LMS algorithm for the anti-noise signal that is also injected into the power splitter. Due to this simple test setup, no special circuits or sensors for sensing or anti-noise injection are necessary. Inside the power splitter setup, the noise and anti-noise signals are superimposed and the residual noise can be measured at the third port of the splitter.

For adapting the notch filter weights, the residual noise signal is measured and evaluated by the delayed LMS algorithm. In parallel, an oscilloscope or an EMI receiver measures the residual noise signal for evaluation purposes.

In the following, the noise and residual noise signals are measured with help of an oscilloscope. Afterward, the FFT of the noise signal is calculated. With help of the previously described parametrization strategy, the adaptive notch filter's step size μ is calculated for three exemplary sidebands around 200 kHz, 1 MHz and 12,5 MHz and different maximum noise levels. Finally, the adaptive notch filter is applied and its efficiency is evaluated.

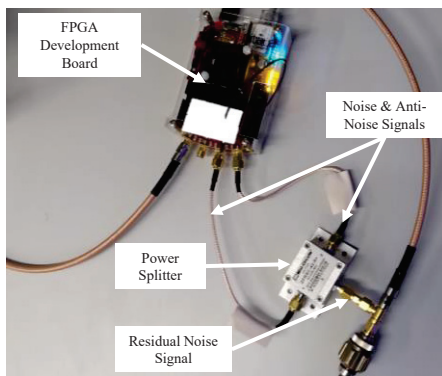


Fig. 10. Photograph of the simple test setup

A. Measurement of the noise spectrum

In a first step the noise signal is measured with an oscilloscope while the adaptive notch filter is turned off. In Fig. 12, three different switching harmonics and sidebands of the noise signal's FFT are depicted (blue). Moreover, three arbitrarily chosen noise limit lines are illustrated in Fig. 12 (green).

B. Parametrization

Based on the calculated noise spectra (step 1) and the determined noise-limit (step 2), the demanded noise reductions are calculated (step 3) and shown in Fig. 11 for the three regarded sidebands. The demanded reduction X_{dB} (step 4) and the demanded notch filter bandwidth B_{XdB} (step 5) are determined. In this special case, the sideband is relatively wide and due to the steep form of the filter notch, the outer sideband harmonics – that are not the sideband harmonics with the highest demanded noise reduction – are determining the notch filter's needed bandwidth B_{XdB} and the demanded reduction X_{dB} , because near to the switching

harmonic (where the filter notch is placed), the noise suppression of the notch filter is high enough. With help of (10), the required notch filter step size μ is calculated (step 6).

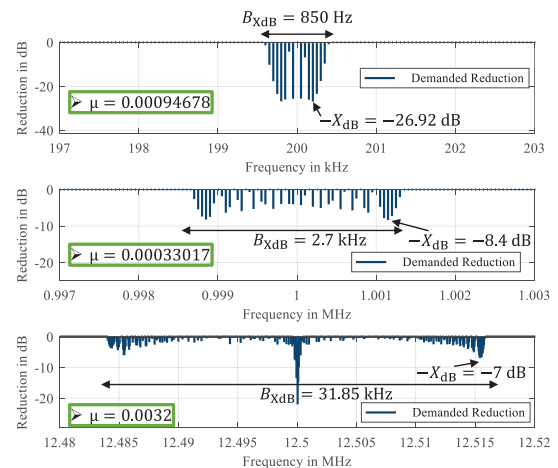


Fig. 11. Demanded noise reductions in dB for the three noise signal sidebands, Calculated corresponding step sizes μ

In the real test setup (in difference to the simulation), the anti-noise signal passes a transmission path between synthesis and interference with the noise signal. In case of the splitter test setup, the resulting residual noise signal is reduced by around 12 dB (factor 0.25), in first proximity. To compensate this attenuation, that is caused by the secondary path, the quadruple step size 4μ has to be chosen.

C. Oscilloscope measurement and FFT

After the needed step sizes are calculated, the noise and residual noise signals are measured with help of an oscilloscope. The afterwards calculated FFTs of the noise and residual noise signals are depicted in Fig. 12. In case of the sidebands around 200 kHz and 1 MHz, the considered sideband harmonics of the residual noise reveal residual noise levels below the arbitrarily demanded limit. In case of the sideband around 12.5 MHz, the sideband harmonics near the switching harmonic exceed the noise limit. This is due to their high noise levels and the relatively large step size 4μ that involves a fast adaptation speed, but also reduces the precision of the cancellation signal. Hence, a compromise between adaptation speed and precision has to be made.

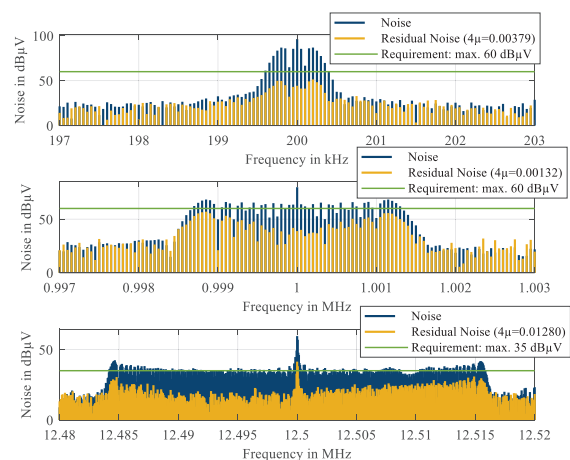


Fig. 12. Comparison of the three (residual) noise sidebands

D. EMI test receiver measurement

In addition, the noise and residual noise signals are measured by an EMI receiver with 9 kHz resolution bandwidth in the frequency range of the considered sidebands. Fig. 13 shows the corresponding noise and residual noise measurements with peak and average detector. All measurements reveal significant noise reductions for the considered switching harmonic and its sidebands. The measurement of the residual noise signal in the frequency range around 12.5 MHz reveals a small amplification, compared to the noise signal measurement. Here, the influence of the error-prone estimation of the secondary path becomes perceptible. As described in, e.g. [18], the noise amplification is caused by a defective secondary path estimation. Noise amplification could be minimized by additional estimation loops but is not implemented yet.

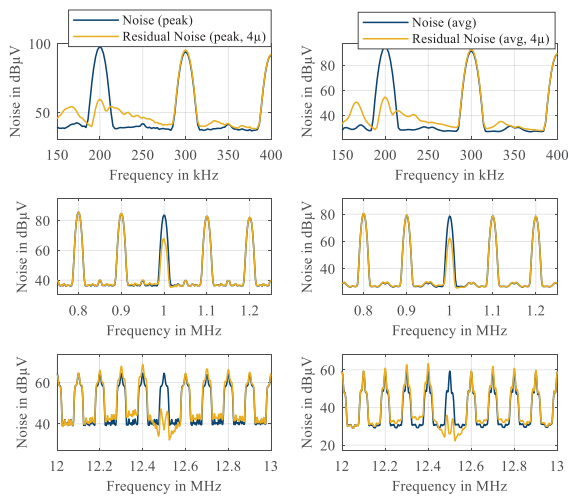


Fig. 13. EMI Receiver measurement (RBW = 9 kHz, peak (left column), average (right column)) of the noise and residual noise signals

VII. CONCLUSION AND OUTLOOK

In this work, adaptive notch filter implementations have been examined regarding their ability to suppress sideband harmonics of PWM-signals. Therefore, an analytical description of the ideal adaptive notch filter's behavior has been summarized that allows a deeper understanding. With help of this analytical description, adaptive notch filter implementations can be parametrized regarding their bandwidth and the needed noise suppression, to a certain extent. The presented parametrization strategy is successfully tested with help of simulations and measurements on a simple test setup that emulates an inverter's pulse-width-modulated switching waveform. The demanded noise reductions up to 27 dB in the sidebands could be realized.

The behavior and the compensation of the secondary path in adaptive notch filter implementations shall be subject of future investigations. Furthermore, overlapping notch filters will be investigated and applied to a real inverter.

REFERENCES

- [1] K. Mainali and R. Oruganti, "Conducted EMI mitigation techniques for switch-mode power converters: A Survey," *IEEE Trans. Power Electron.*, vol. 25, no. 9, pp. 2344-2356, Sep. 2010.
- [2] "CISPR 25 – Vehicles, boats and internal combustion engines – Radio disturbance characteristics – Limits and methods of measurement for the protection of on-board receivers," 4th ed., Feb. 2015.
- [3] Y.-C. Son and S.-K. Sul, "Generalization of active filters for EMI reduction and harmonics compensation," *IEEE Trans. Ind. Appl.*, vol. 42, no. 2, pp. 545-551, Mar.-Apr. 2006.
- [4] N. K. Poon, J. C. P. Liu, C. K. Tse and M. H. Pong, "Techniques for input ripple current cancellation: classification and implementation [in SMPS]," *IEEE Trans. Power Electron.*, vol. 15, no. 6, pp. 1144-1152, Nov. 2000.
- [5] B. Narayanasamy and F. Luo, "A survey of active EMI filters for conducted EMI noise reduction in power electronic converters," *IEEE Trans. Electromagn. Compat.*, vol. 61, no. 6, pp. 2040–2049, Dec. 2019.
- [6] A. Bendicks, "Active Cancellation of Electromagnetic Emissions of Power Electronic Systems by Injecting Synthesized and Synchronized Signals," Ph.D. dissertation, On-board Systems Lab, TU Dortmund University, Dortmund, Germany, 2020. [Online]. Available: <https://eldorado.tu-dortmund.de/handle/2003/39212?locale=en>.
- [7] A. Bendicks, M. Rübartsch and S. Frei, "Simultaneous EMI Suppression of the Input and Output Terminals of a DC/DC Converter by Injecting Multiple Synthesized Cancellation Signals," in *Proc. Int. Symp. Electromagn. Compat. Eur.*, Barcelona, Spain, 2-6 Sep. 2019, pp. 842-847.
- [8] S. M. Kuo and D. R. Morgan, "Active Noise Control: A Tutorial Review," *Proc. IEEE*, vol. 87, no. 6, pp. 943-973, Jun. 1999.
- [9] A. Bendicks, T. Dörlemann, S. Frei, N. Hees and M. Wiegand, "Development of an Adaptive EMI Cancellation Strategy for Stationary Clocked Systems," in *Proc. Int. Symp. Electromagn. Compat. Eur.*, Amsterdam, Netherlands, 27-30 Aug. 2018, pp. 78-83.
- [10] A. Bendicks, A. Peters, S. Frei, M. Wiegand, N. Hees, "FPGA-basierte aktive Unterdrückung der elektromagnetischen Störungen einer aktiven Leistungsfaktorkorrektur (PFC) durch die Injektion von modulierten Sinussignalen," in *Proc. Conf. Electromagn. Compat.*, Cologne, Germany, pp. 433-442, 17-19 March 2020.
- [11] A. Bendicks, A. Peters, S. Frei, "FPGA-based Active Cancellation of the EMI of a Boost Power Factor Correction (PFC) by Injecting Modulated Sine Waves," *IEEE Letters on Electromagnetic Compatibility Practice and Applications*, vol. 3, no. 1, pp. 11-14, March 2021.
- [12] T. Dörlemann, A. Bendicks, S. Frei, "Active EMI Suppression with Adapted Cancellation Signals for a Buck Converter in Varying Modes of Operation," in *Proc. PCIM Europe 2021*, Nuremberg, Germany, pp. 879-886, 3-7 May 2021.
- [13] A. Bendicks, T. Dörlemann, S. Frei, N. Hees and M. Wiegand, "Active EMI Reduction of Stationary Clocked Systems by Adapted Harmonics Cancellation," *IEEE Trans. Electromagn. Compat.*, vol. 61, no. 4, pp. 998-1006, Aug. 2019.
- [14] B. Widrow et al., "Adaptive noise cancelling: Principles and applications," *Proc. IEEE*, vol. 63, no. 12, pp. 1692-1716, Dec. 1975.
- [15] J. R. Glover, "Adaptive noise canceling applied to sinusoidal interferences," *IEEE Trans. Acoust., Speech, Signal Process.*, vol. 25, no. 6, pp. 484-491, Dec. 1977.
- [16] S. M. Kuo and D. R. Morgan, "Active Noise Control Systems – Algorithms and DSP Implementations," New York: Wiley, 1996.
- [17] E. Ziegler, Jr., "Selective active cancellation system for repetitive phenomena," U.S. Patent 4 878 188, 31 Oct. 1989.
- [18] S. M. Kuo, X. Kong, S. Chen, "Out-of-Band Overshoot in Narrowband Active Noise Control Systems," in *Proc. Int. Conf. Signal Process. (ICSP)*, Beijing, China, pp. 474-477, 12-16 Oct. 1998.